Silicon (2023) 15:3365–3378
https://doi.org/10.1007/s12633-022-02249-7

ORIGINAL PAPER

Effect of Addition of Dysprosium Oxide on Spectroscopic Properties and Judd–Ofelt Analysis of Lithium Borosilicate Glass System

I. Kashif[1] · **A. Ratep**[2]

Received: 3 October 2022 / Accepted: 28 November 2022 / Published online: 20 December 2022

Abstract

The lithium borosilicate glass containing Dy_2O_3 was prepared by the melt quenching technique. Due to an increase in Dy^{3+}, the intensity of bands increases, they get wider, and they contain a combination of bands, according to infrared data analysis. Several absorption peaks can be seen in the optical absorption spectrum of glass samples, but a strong absorption peak can be seen in the (Near Infrared) NIR area at wavelengths of 1250 nm. The optical intensity rises with Dy_2O_3 content until it reaches 1.5 mol% Dy_2O_3, at which point it drops. The trend in Judd–Ofelt parameters is $\Omega_2 > \Omega_6 > \Omega_4$. The asymmetry between Dy^{3+} ions and the ligand field environment in the glass samples is stronger in the present work than in previously reported Dy^{3+} doped glasses, showing a higher asymmetry between Dy^{3+} ions and the ligand field environment in the glass samples. Excitation wavelengths of 350 nm, 370 nm, and 390 nm were used to create luminescence emission spectra. Both glasses excited at 370 nm and 390 nm showed quenching at 0.5 mol %, while samples stimulated at 350 nm showed quenching at 0.1 mol%, Dy_2O_3. The Y/B values of the prepared glass samples under investigation are around 1, indicating that white light production is possible. The figure of Ω_4/Ω_6 suggested that laser production would be possible. All the samples are lit in a near-perfect white light (0.33, 0.33). CCT, which measures illumination appearance and white light chromaticity, was used to investigate color purity and associated color temperature (CCT).

Keywords XRD · FTIR · Judd Ofelt theory · Optical properties · Warm white light

1 Introduction

Saving energy and reducing the area of the form used for lighting is becoming a growing priority around the world. To draw the attention of a solid-state (SSL) light, this design originated from a mercury argon discharge fluorescence lamp [1–3]. SSL is made up of W-LEDs that are activated by a UV or violet chip and are created from an InGaN blue LED chip that has been coated with a crystalline YAG: yellow phosphorous or RGB phosphor [4–6].

When working with phosphors to make W-LEDs, a variety of issues arise, including white light scattering, a low color rendering index, a high associated color temperature, and lighting degradation. It produces poor heat resistance, which reduces the light intensity and alters the emission color [4, 7–9]. Researchers are working hard to eliminate this flaw by replacing the phosphor with a material that is both thermally stable and light dispersive.

Silicon-based materials are used in manufacturing instead of phosphor to decrease the defect that has been related to a slew of difficulties, including longer and more expensive production [8]. Glass is preferred over crystalline materials. With the physical properties and high solubility of (rare earth) RE ions that allow it a wide emissivity and wavelength tenability, it is a more complete fabrication, easier to shape, and decorate any shape [9].

It is preferred to make an alkaline borosilicate glass doped with Dy^{3+} because of its multiple advantages. To begin with, silicate is transparent, thermally stable, and has high phonon energy [8]. The borate has a boron valence of + 3, has a low melting temperature, is suitable for glass forming, has a low heat fusion temperature, and has a low heat fusion temperature [4, 10–12]. In addition, the two formers have high RE solubility and excellent heat stability [13].

✉ I. Kashif
ismailkashif52@yahoo.com; ismailkashif@azhar.edu.eg

[1] Physics Department, Faculty of Science, Al-Azhar University, Cairo 11884, Nasr City, Egypt

[2] Department of Physics, Faculty of Women for Art, Science & Education, Ain Shams University, Cairo 11757, Heliopolis, Egypt

The addition of alkali can result in a decrease in phonon energy, resulting in high emission efficiency, as well as a change in the former's coordination number, leading to changes in the physical properties of the glass formed [4, 14].

Dy ions were chosen because their frequency range differed from that of other ions. Blue emission ($^4F_{9/2} \rightarrow {}^6H_{15/2}$) at 483 nm, which is used in the contact amplifier [15, 16], and yellow emission ($^4F_{9/2} \rightarrow {}^6H_{13/2}$) at 575 nm, which is highly dependent on host type and Dy^{3+} concentration [17, 18], characterize the visible area. To adjust the white emission, change the Y/B ratio [8].

Dy^{3+} symmetry is also explained in terms of the covalent link between Dy and the oxygen ion [4]. Several studies have investigated the effects of doping Dy^{3+} in various formers. Several researchers [1, 19–22] investigated the effects of Dy^{3+} doping on the structural, physical, optical, luminescent, and thermos-luminescent properties of various formers. The effect of substituting Dy_2O_3 for B_2O_3 on the optical characteristics and radiation originating from the stimulation of lithium borosilicate samples was investigated [23]. According to the authors, CIE coordinate values are declining in the white light zone. The CCT values of the samples under investigation suggest that, under the appropriate excitation, cold light can be generated from the produced glass. As a result, some of the glass samples under investigation could be suited for ambitious projects involving laser and cool white light development.

The purpose of the study is to see how different amounts of Dy_2O_3 affect the structure of borosilicate glass samples, as well as their optical properties and white light emission.

2 Experimental Works

The glass sample's composition of 30 SiO_2 + 35 Li_2O + 35 B_2O_3 + x Dy_2O_3 where x = 0.1, 0.5, 1, 1.5, and 2 mol% were melted in a porcelain crucible at 1100 °C for half an hour before being poured between two copper plates in an electric muffle furnace, (Lenton).

The X-ray diffraction (XRD) technique was used to determine the nature of the investigated substances (Philips Analytical type PW3710).

The Archimedes method is used to calculate the density of glass samples.

$$\rho = \frac{\rho_t W_a}{(W_a - W_b)} \text{gcm}^{-3} \quad (1)$$

The weights of glass samples in air and toluene, respectively, are W_a and W_b, and ρ_t is the density of toluene (ρ_t = 0.865 g cm^{-3}).

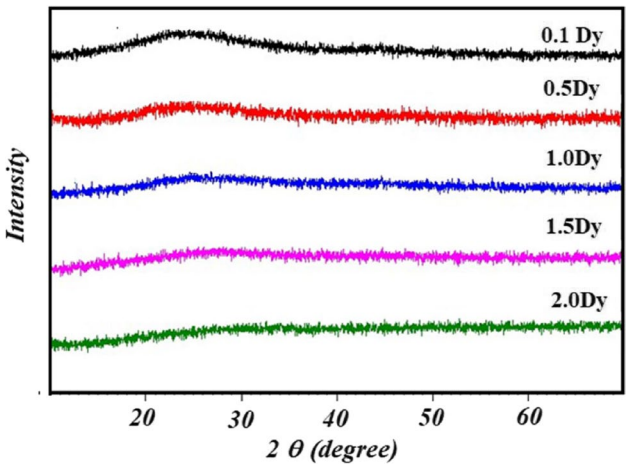

Fig. 1 The X- ray diffraction of the prepared glass samples

The vibration groups of the studied samples were investigated using the KBr disc technique in the range of 2000–400 cm^{-1} using a JASCO FTIR-4100.

The optical absorption spectra in the range of 190 to 2500 nm were measured using a computerized recording spectrophotometer (JASCO 570).

The emission was measured using a spectrofluorometer (JASCO FP-6300) in the wavelength range of 200–800 nm.

3 Results and Discussion

3.1 Structure Properties

Figure 1 depicts the XRD pattern of prepared glass samples. The presence of a broad hump and the absence of distinct peaks indicate that the samples are amorphous.

The infrared spectra of lithium borosilicate glass samples containing Dy^{3+} ions are shown in Fig. 2. The B–O

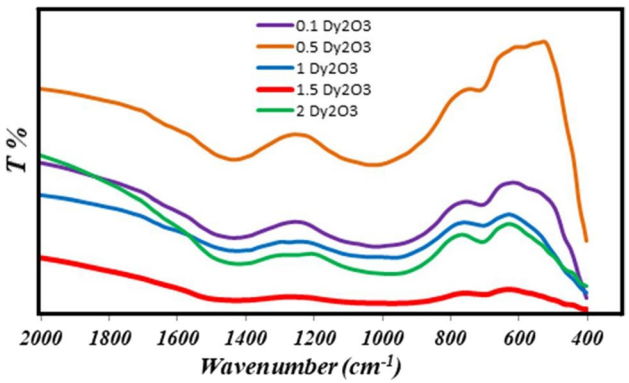

Fig. 2 The infrared spectra of lithium borosilicate glass samples containing Dy^{3+} ions

stretching vibrations of trigonal $(BO_3)^{3-}$ units (in meta-, pyro-, and ortho-) are responsible for the broadband of 1200–1700 cm^{-1} (centered at 1376 cm^{-1}). Anti-symmetrical stretching vibrations with three NBOs of B–O–B groups were assigned to the band at 1420–1540 cm^{-1} [24].

The stretching vibrations of the non-bridged oxygen atom (O–B–O) in the $[BO_2O]^-$units interconnected with $[BO_4]$ units or $[BO_3]$ units are located at 1360 cm^{-1} and 1455 cm^{-1}, respectively [25]. Increases in Dy^{3+} concentration increase band intensity while decreasing 1280–1600 cm^{-1} bandwidth. The absence of the band at 1214 cm^{-1} implies asymmetric stretching of ortho-borate B-O bonds [22].

The band at 1228 cm^{-1} [25] is due to symmetric bonds from B–O, a stretch of pyroborate units $[B_2O_5]^{4-}$.

As the intensity of the band at 800–1200 cm^{-1} grows, it widens and becomes wider. The stretching vibrations of B–O bonds in tetrahedral BO_4 units cause Dy^{3+} to include a combination of bands, constructed from two bands at 886 and 928 cm^{-1}.

The non-bridging oxygen (NBOs) vibration in the form of the BO_4 group is responsible for the band around 1005 cm^{-1}. The stretching vibration of B–O–M causes the band at 995 cm^{-1}. Overlapping contributions of silicate and borate groups containing BO_3 and BO_4 units can occur when silicate and borate groups in the 1000–1120 cm^{-1} range are overlapping [22, 26]. From the stretching vibrations of Si–O–Si bonds, the possible configurations of existence in the glassy network for silicates [8] are Q3 (1075 cm^{-1}) (3 bridging oxygen and one non-bridging), Q2 (1000 cm^{-1}) (2 bridging oxygen and 2 non-bridging), and Q1 (900 cm^{-1}) (1 bridging oxygen and 3 non-bridging). The presence of B-O-Si bonds accounts for the band at 1020 cm^{-1}. The stretching vibration of Si–O–Si bonds in the NBO of SiO_4 tetrahedral units causes two bands at 1040 and 1100 cm^{-1}. That is, as the NBO bonds (Si–O–Si links in Q1 units) rose, so did the bridge oxygen bond (Si–O–Si bonds) [24].

The bending vibration in symmetric BO_3, the bending vibrations of Si–O–B bridges, the presence of BO_4 vibration tetrahedral units, and the symmetrical bending of the Si–O–Si vibration group [27] are all covered by the band at 688 cm^{-1} [27, 28]. The emergence of a band at 455 cm^{-1} [26] when Dy concentration increases was attributed to the deformation vibration of bonds in Si–O groups, including SiO_4 tetrahedra overlapped with B–O–B linkages, as well as the vibration of a metal cation such as Li^+ peaks [22, 28–30]. According to the results, silicate groups grow at the expense of BO_3 groups, which explain the rise in the Si–O-B bonding connection.

3.2 Physical Properties

From the perspective of bridging oxygen BO and NBOs, density plays an important role in characterizing the glass structure.

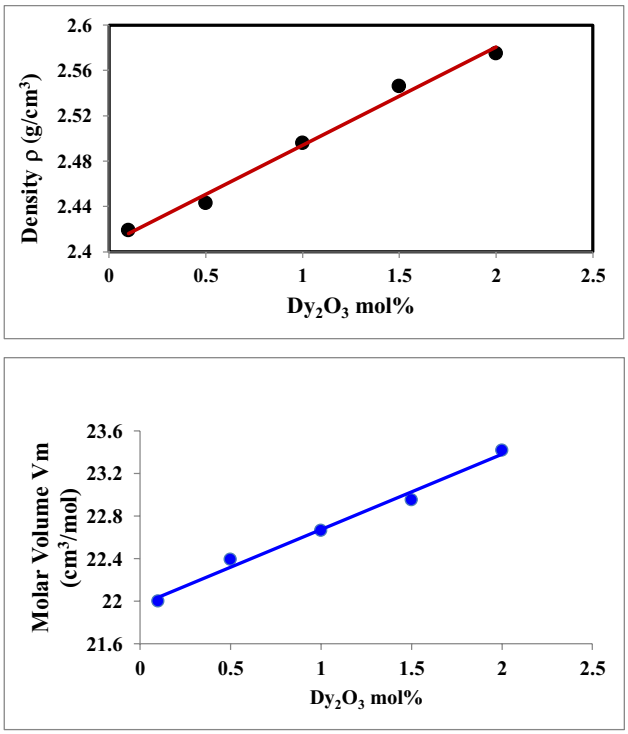

Fig. 3 The effect of Dy content on the density and molar volume

The effect of Dy_2O_3 concentration on density and molar volume is seen in Fig. 3. The density ρ and molar volume Vm {Molar volume = molecular weight/ density (Vm = Mw/ρ)} exhibit a similar tendency in this picture, with the density and Vm increasing as the Dy_2O_3 concentration increases. Dy^{3+} enters the interstitial position in the glass structure, breaks bonds to create NBOs, and causes a volume increase [27, 31]. The density increased as the MW (molecular weight) of Dy increased [32, 33]. Vm increases as the oxygen level rises, resulting in the de-polymerization of glass structures [34, 35].

3.3 Optical Properties

The optical band gap is important in photonic applications [20] because it allows for a visual representation of the levels between the valance and conduction bands. The optical band gap Eg was calculated using Tauc plots and the absorption coefficient approach (α) based on the relationship between $(\alpha h\nu)^2$ and $h\nu$ [33].

In Fig. 4, the optical band gap values are calculated and depicted.

The Eg value drops until it reaches 0.5 mol % Dy_2O_3 and then rises. The ionic character acquired from NBOs reduces Eg, which increases localized state-formed bonding defects [28, 32, 36–39].

Many researchers investigated the effects of changing parameters on the optical band gap, such as modifier concentrations [29], boron substitution with Dy [25, 31], and

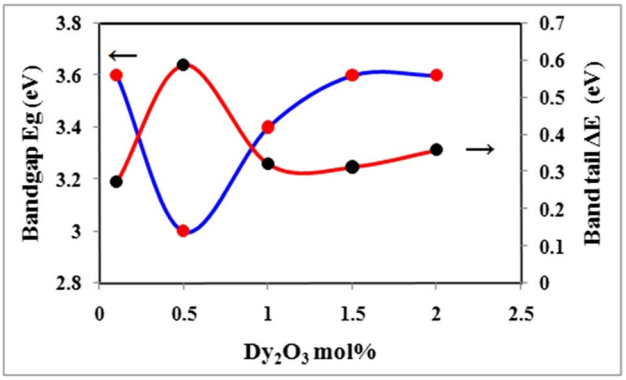

Fig. 4 The effect of Dy_2O_3 concentration on the optical band gap and band tail

an intermediate like Al substitution with Dy [20], and all concluded that an increase in Dy_2O_3 concentration leads to a decrease in Eg values. The Urbach relation, according to [35], defines the degree of disorder.

$$\alpha(\upsilon) = \alpha o \exp\left(\frac{h\upsilon}{\Delta E}\right) \tag{2}$$

where αo is a constant and ΔE is the band tail, computed from the linear relationship between ln(α) and hυ.

From the relation between ln (α) and hυ observed the reverse behavior between Eg and ΔE, and the sample containing 0.5 mol% Dy_2O_3 has the highest value of defects and a drop in the amorphous semiconductor ratio [34].

The optical absorption spectra of Dy-doped glass samples (Fig. 5) reveal the transition area, kind of transition, line strength, and structure. Figure 5 shows that as the Dy_2O_3 content increases up to 1.5 mol%, the absorption increases, and then drops.

Figure 5 shows the transition of Dy [40] from the ground state $^6H_{15/2}$ to the excited level $^6P_{7/2}$, $^4I_{15/2}$, $^4F_{9/2}$, $^6F_{3/2}$, $^6F_{5/2}$, $(^6F_{7/2}+{}^6H_{5/2})$, $(^6F_{9/2}+{}^6H_{7/2})$, $(^6F_{11/2}+{}^6H_{9/2})$ and $^6H_{11/2}$ at 348, 426, 450, 746, 792, 880,1068, 1246, and 1672 nm, respectively.

High optical absorption intensity at 1260 nm, hypersensitive transition, which follows the selection rules $|\Delta S| = 0, |\Delta L| \leq 2 and |\Delta J| \leq 2$ [40], and mostly impacts the environment. And the low intensity appears in the visible region according to the forbidden transition [4].

3.4 Judd–Ofelt Parameters

According to the relationship presented in ref [9, 23], the form of the optical absorption band is used to determine the line strength experimentally.

Line strength experimentally

$$(f_{exp}) = 4.32x10^{-9} \int \alpha(v)dv \tag{3}$$

The integrated area under the peak might be used to figure it out. The line's strength was determined using the reference's relation [4, 23] and listed in Table 1.

The Root mean square deviation δ_{rms} [40] determines the fit between experimentally acquired f_{exp} and estimated f_{calc} values.

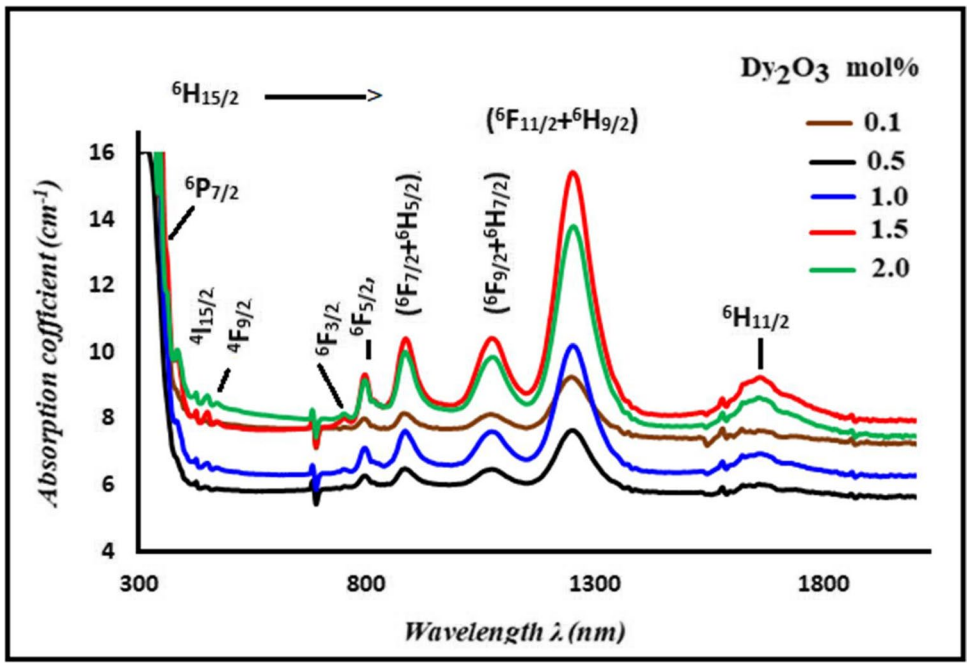

Fig. 5 Optical absorption spectra of glass samples doped with Dy^{3+}

Table 1 Experimental, calculated line strength and the root mean square deviation for all prepared glass samples

$_{nm}\lambda$	2 Dy_2O_3		1.5 Dy_2O_3		1 Dy_2O_3		0.5 Dy_2O_3		0.1 Dy_2O_3	
	f_{cal}	f_{exp}	f_{cal}	f_{exp}	f_{cal}	f_{exp}	f_{cal}	f_{exp}	f_{cal}	f_{exp}
1246	48.8	48.9	79.5	79.5	62.6	58.1	58.7	58.7	288	287
1068	9.64	8	15.6	12.8	0.119	9.97	11.5	11	54.9	32.3
880	6.70	8.75	10.9	13.8	8.67	0.11	8.53	11.4	36.3	42.9
792	5.41	4.63	7.34	7.24	6.95	5.90	11.2	5.9	33.2	19.8
746	0.22	0.86	0.37	1.36	0.17	1.11	0.16	1.11	1.04	3.71
450	0.28	2.54	0.47	4.04	0.38	3.25	0.38	3.14	2.07	12
426	0.158	0.089	0.21	0.159	0.118	0.099	0.16	0.158	1.38	1.65
348	0.73	4.98	0.99	8.48	0.65	5.68	-----	------	-----	-----
δ_{rms}	3.02		5.33		1.68		0.34		8.79	
Error%	6.21		6.72		2.69		0.58		3.06	
Ω_4/Ω_6	0.078		0.105		0.044		0.186		0.86	

$$\delta_{rms} = \sqrt{\frac{\sum(f_{exp} - f_{calc})^2}{N-3}} \tag{4}$$

where N is the number of energy transition levels.

And [41] is used to measure the proportion of relative error:

$$\text{Error\%} = \frac{\text{root mean square}}{F_{\exp\, max} - F_{\exp\, min}} \tag{5}$$

$F_{exp\ max}$ and $F_{exp\ min}$ are the maximum (hypersensitive transition) and minimum experimental oscillator forces, respectively.

All the results show an excellent match between experimental and computed values.

All the determined peak intensities except the peak $^6H_{15/2}$-$^6H_{11/2}$ in all glass samples and the band 348 nm in glass samples concentrations of 0.1 and 0.5 mol% Dy_2O_3 were calculated using the Judd Ofelt parameters Ω_2, Ω_4, and Ω_6.

The influence of Dy_2O_3 concentration on the Judd Ofelt parameters is seen in Fig. 6. The trend in the Judd–Ofelt parameters is $\Omega_2 > \Omega_6 > \Omega_4$.

Table 2 shows the JO parameters that were acquired.

The Judd–Ofelt parameter intensities values of the glass samples under study are higher than the other glass systems, and follow the trend $\Omega_2 > \Omega_6 > \Omega_4$, suggesting that Dy^{3+} was successfully doped in the glass matrix, according to Table 2.

According to Table 2, the Judd–Ofelt parameter intensities values of the glass samples under study are higher than the other glass systems and follow the trend $\Omega_2 > \Omega_6 > \Omega_4$, indicating that Dy^{3+} was successfully doped in the glass matrix.

The larger Ω_6 than Ω_4 values are explained by the host's influence with varying concentrations of rare-earth ions [34].

The asymmetry of the ligand field environment surrounding the RE^{3+} ion site and the covalency of the metal–ligand bond are both influenced by the Ω_2 values.

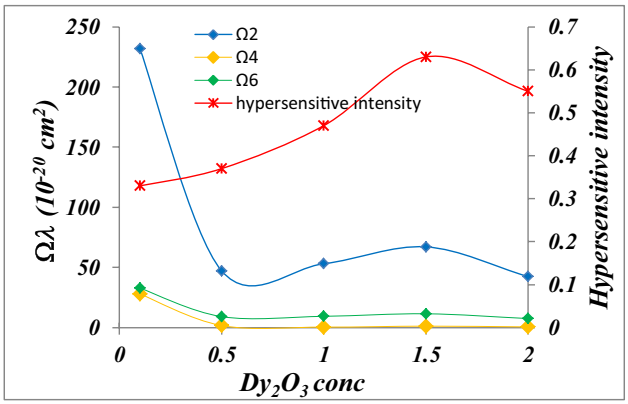

Fig. 6 The effect of Dy content on the Judd Ofelt parameters

Higher values of Ω_2 imply that the dysprosium ions and oxygen ions in Dy_2O_3 are more covalent, as well as the asymmetry of Dy^{3+} ions.

The Ω_2 parameter, which affects the covalence of rare-earth ions, impacts the sensitivity of the rare-earth matrix, ligand anions, and site symmetry, whereas the viscosity and hardness of the host glass matrix are related to Ω_4 and Ω_6 [20]. As a result, the greatest value of Ω_2 confirms that rare-earth Dy^{3+} ions have greater covalence, surrounding ligands, and site symmetry. As a result, a high-quality host glass matrix for optical and lightning device applications has been confirmed [21].

The JO intensity parameters provide information on the type of ligand-RE^{3+} ion bonds as well as RE^{3+} ion site symmetry.

Short-range effects are represented as the valence of the RE–O bond and are dependent on hypersensitivity transitions, hence the parameter Ω_2 is utilized to calculate the coordination structure asymmetry.

However, the long-range effect factors Ω_4 and Ω_6 are summarized in defining bulk properties [4]. The high value of Ω_2 indicates a high covalency and reduces Dysprosium's coordination symmetry.

Table 2 The J-O intensity parameters Ω_λ ($\times 10^{-20}$ cm^2) of prepared glass samples (comparison with other glass references), and Ω_4/Ω_6 ratio

Glass composition	Ω2	Ω4	Ω6	trend	Ω4/Ω6	Reference
lithium borosilicate glass 0.1Dy	290	31.4	42.3	Ω2 > Ω6 > Ω4	0.74	P. w
lithium borosilicate glass 0.5	59.11	1.011	12.036	Ω2 > Ω6 > Ω4	0.084	P. w
lithium borosilicate glass 1.0	66.019	0.247	11.913	Ω2 > Ω6 > Ω4	0.021	P. w
lithium borosilicate glass 1.5	83.299	1.253	14.582	Ω2 > Ω6 > Ω4	0.086	P. w
lithium borosilicate glass 2.0	52.582	0.525	9.557	Ω2 > Ω6 > Ω4	0.055	P. w
Bismuth-based fluorophosphate glasses 1Dy	10.05	4.28	3.09	Ω2 > Ω4 > Ω6	1.385	[42]
lead borate titanate aluminum fluoride: Dy3 +	7.05	1.22	1.91	Ω2 > Ω4 > Ω6	0.639	[43]
niobium containing tellurium calcium zinc borate: Dy^{3+}	11.3	3.3	2.6	Ω2 > Ω4 > Ω6	1.269	[44]
Dy: Potassium lead tellurofluoroborate glasses	9.86	3.39	2.41	Ω2 > Ω4 > Ω6	1.407	[45]
Tellurite	8.59	1.48	2.43	Ω2 > Ω4 > Ω6	0.609	[46]
Bismuth fluoro phosphate	11.21	1.63	3.12	Ω2 > Ω4 > Ω6	0.522	[47]
1.0 Dy: bismuth phosphate glasses	13.91	5.97	3.04	Ω2 > Ω4 > Ω6	1.964	[48]
Oxyfluoro borate	19.9	4.52	9.21	Ω2 > Ω4 > Ω6	0.491	[9]
magnesium-sodium-borotellurite glasses 0.05	30.86	5.78	4.44	Ω2 > Ω4 > Ω6	1.302	[49]
magnesium-sodium-borotellurite glasses 0.5	35.98	8.87	2.12	Ω2 > Ω4 > Ω6	4.184	[49]
magnesium-sodium-borotellurite glasses 1.0	33.54	7.8	5.07	Ω2 > Ω6 > Ω4	1.538	[49]
magnesium-sodium-borotellurite glasses 1.5	21.09	1.69	7.49	Ω2 > Ω6 > Ω4	0.226	[49]
Lithium borosilicate 1.0Dy	52.8	0.775	10.6	Ω2 > Ω6 > Ω4	0.073	[23]
Lithium borosilicate 2.50Dy	46.6	5.33	7.26	Ω2 > Ω6 > Ω4	0.734	[23]
Lithium borosilicate 5.0Dy	37	5.62	5.69	Ω2 > Ω6 > Ω4	0.988	[23]
Lithium borosilicate 10.0Dy	40.7	7.9	5.55	Ω2 > Ω4 > Ω6	1.423	[23]
Tellurite	16	2.39	3.75	Ω2 > Ω4 > Ω6	0.637	[50]
Germanate	3.65	0.65	1.57	Ω2 > Ω6 > Ω4	0.414	[51]
Tellurite	1.46	2.32	3.6	Ω6 > Ω2 > Ω4	0.367	[52]
Borate	23.02	12.86	12.17	Ω2 > Ω4 > Ω6	1.057	[53]
Aluminoborosilicate Dy 0.1	12.59	0.45	17.52	Ω6 > Ω2 > Ω4	0.026	[31]
Molybdenum borosilicate0.98	0.98	0.23	0.69	Ω2 > Ω4 > Ω6	0.333	[54]
Silicate	8.32	2.14	2.75	Ω2 > Ω6 > Ω4	0.778	[18]
Lead borosilicate	11.43	4.38	3.82	Ω2 > Ω4 > Ω6	1.147	[55]
Phosphate	8.05	2.77	2.31	Ω2 > Ω4 > Ω6	1.199	[56]
Silicate	8.06	2.24	2.03	Ω2 > Ω4 > Ω6	1.103	[57]
Potassium lead bismuth borate (K1Dy)	5.28	2.77	1.64	Ω2 > Ω4 > Ω6	1.689	[58]
Sodium lead bismuth borate (Na1Dy)	5.79	1.78	1.77	Ω2 > Ω4 > Ω6	1.006	[58]
Calcium lead bismuth borate (Ca1Dy)	5.78	1.66	1.62	Ω2 > Ω4 > Ω6	1.025	[58]
Strontium lead bismuth borate (Sr1Dy)	5.07	2.18	1.8	Ω2 > Ω4 > Ω6	1.211	[58]
Barium lead bismuth borate (Ba1Dy)	5.2	2.9	1.46	Ω2 > Ω4 > Ω6	1.986	[58]
Dy: bismuth zinc borate glasses	4.03	1.14	1.65	Ω2 > Ω6 > Ω4	0.691	[59]
Dy: zinc-lithium- borotellurite glasses	4.42	1.2	1.18	Ω2 > Ω4 > Ω6	1.017	[60]
Dy: Barium Borophosphate	4.71	1.27	0.99	Ω2 > Ω4 > Ω6	1.283	[61]
1Dy: sodium bismuth strontium phosphate glasses	2.48	0.82	0.61	Ω2 > Ω4 > Ω6	1.344	[62]
Dy: yttrium calcium silicoborate glasses	2.84	0.15	0.95	Ω2 > Ω6 > Ω4	0.158	[63]
Dy: fluoroaluminatetellurite	3.02	0.77	2.01	Ω2 > Ω6 > Ω4	0.383	[64]
Lithium boro-tellurite: Dy	12.05	1.22	0.76	Ω2 > Ω4 > Ω6	1.57	[65]
Calcium boro-tellurite: Dy	11.88	1.19	0.75	Ω2 > Ω4 > Ω6	1.59	[65]
Zinc boro-tellurite: Dy	14.24	2.4	0.96	Ω2 > Ω4 > Ω6	2.55	[65]
Barium boro-tellurite: Dy	12.24	1.28	0.78	Ω2 > Ω4 > Ω6	1.6	[65]
Strontium boro-tellurite: Dy	14.09	2.13	0.88	Ω2 > Ω4 > Ω6	1.95	[65]
Boro-tellurite glasses	8.05	1.2	1.02	Ω2 > Ω4 > Ω6	1.18	[66]
Lithium potassium borate	25.68	0.28	3.18	Ω2 > Ω6 > Ω4	0.09	[67]
Bi2O3-B2O3-Ga2O3-GeO2-TeO2 0.5 Dy	25.4	10.1	3.12	Ω2 > Ω4 > Ω6	3.24	[68]

Table 2 (continued)

Glass composition	Ω2	Ω4	Ω6	trend	Ω4/Ω6	Reference
1.0 Dy	32.7	7.54	4.96	Ω2 > Ω4 > Ω6	1.52	[68]
1.5 Dy	34.2	1.78	7.78	Ω2 > Ω4 > Ω6	4.37	[68]
2.0 Dy	34.8	2.19	7.74	Ω2 > Ω6 > Ω4	3.53	[68]
SiO2–B2O3–Al2O3–NaF–ZnF2: Dy0.5	2.026	1.111	1.849	Ω2 > Ω6 > Ω4	0.601	[30]
: Dy 0.7	1.329	0.564	1.003	Ω2 > Ω6 > Ω4	0.562	[30]
: Dy 1.0	2.437	0.606	1.989	Ω2 > Ω6 > Ω4	0.305	[30]
: Dy 1.5	1.594	0.541	0.654	Ω2 > Ω6 > Ω4	0.827	[30]
calcium boroaluminate glasses : Dy	5.247	0.116	2.1	Ω2 > Ω6 > Ω4	0.055	[69]
Zinc calcium tellurofluoroborate glasses: Dy	6.245	1.8241	2.8002	Ω2 > Ω6 > Ω4	0.651	[70]
Potassium aluminum telluroborate glasses**: Dy**	3.34	0.2	0.68	Ω2 > Ω6 > Ω4	0.294	[71]
Dy: Zinc Alumino Bismuth Borate glasses	2.23	0.14	0.41	Ω2 > Ω6 > Ω4	0.341	[72]
Dy: B2O3-PbO-Al2O3-ZnO glasses	7.321	2.567	2.807	Ω2 > Ω6 > Ω4	0.914	[4]
Sodium lead alumino borosilicate Dy 0.5	7.535	2.088	2.311	Ω2 > Ω6 > Ω4	0.903	[20]
Sodium lead alumino borosilicate Dy 1.0	14.495	1.264	2.234	Ω2 > Ω6 > Ω4	0.567	[20]
Sodium lead alumino borosilicate Dy 1.5	10.322	1.573	3.517	Ω2 > Ω6 > Ω4	0.447	[20]
Oxy-fluoroborate glasses: Dy10	16.3	6.99	7.28	Ω2 > Ω6 > Ω4	0.95	[9]
lead telluroborate glasses, Dy10	7.75	2.31	2.7	Ω2 > Ω6 > Ω4	0.85	[73]
mixed alkali borate glasses Dy8	13.97	0.51	3.28	Ω2 > Ω6 > Ω4	0.15	[74]
lead lithium fluoroborate glasses: Dy	14.4	5.23	5.71	Ω2 > Ω6 > Ω4	0.92	[75]
sodium lead borophosphate glasses: Dy	6.37	0.34	2.16	Ω2 > Ω6 > Ω4	0.157	[76]
lead fluorophosphates glasses: Dy10	7.12	1.59	2	Ω2 > Ω6 > Ω4	0.795	[77]
B_2O_3-TeO_2-PbO-PbF_2-Bi_2O_3-CdO glasses: Dy	10.216	1.731	2.127	Ω2 > Ω6 > Ω4	0.814	[78]
tellurite based tungsten-zirconium glasses: Dy10	6.91	0.99	1.01	Ω2 > Ω6 > Ω4	0.980	[79]
Na2O–MgO–Bi2O3-B2O3: Dy1.0	26.22	3.43	6.63	Ω2 > Ω6 > Ω4	0.517	[80]
Na2O–BaO–Bi2O3-B2O3: Dy1.0	13.36	7.73	2.01	Ω2 > Ω6 > Ω4	3.846	[80]
Li2O-Gd2O3-Bi2O3- B2O3 glasses: Dy1.0	10.64	6.1	5.86	Ω2 > Ω6 > Ω4	1.041	[81]
Fluorogermanate: Dy	5.41	1.89	1.92	Ω2 > Ω6 > Ω4	0.984	[82]
Sodium fluoroborate: Dy	12.98	3.07	3.74	Ω2 > Ω6 > Ω4	0.821	[83]
lead telluroborate glasses: Dy	7.75	2.31	2.7	Ω2 > Ω6 > Ω4	0.856	[73]
tellurite tungsten-zirconium glasses: Dy	6.91	0.99	1.01	Ω2 > Ω6 > Ω4	0.980	[79]
lead borate glasses: Dy**10**	4.9	0.94	2.07	Ω2 > Ω6 > Ω4	0.454	[84]
fluorozirconate glass: Dy	3.22	1.35	2.38	Ω2 > Ω6 > Ω4	0.567	[85]

Figure 6 indicates the Ω_2 values of glass samples in the same phase as the hypersensitive intensity, although it has a different trend in a sample containing 0.1 Dy_2O_3, which has a high value of Ω_2.

The JO parameters of the investigated glass samples were compared to those of other glass samples prepared as given in Table 3. It noticed the high value of the current glass.

Judd–Ofelt parameters predict the spectroscopic ratio from connection Ω_4/Ω_6 [4, 39]. The obtained value varied according to the Dy_2O_3 content, and a high value for the sample containing 0.1 Dy_2O_3 indicated that laser production was feasible.

Table 2 shows the Ω_4/Ω_6 ratio for the glass samples under investigation compared to other glass systems. The spectroscopic quality factor Ω_4/Ω_6 is a crucial characteristic of a laser's activity, and if it is greater than 0.9, it indicates that the laser is suitable for use.

3.5 Excitation and Emission Properties

Figure 7 shows the excitation of the sample containing 1 mol% Dy_2O_3 in the range from 300 to 500 nm by observing the emission spectra at 575 nm.

From Fig. 7, it observed seven peaks presented at 324 nm, 350 nm, 365 nm, 386 nm, 424 nm, 451 nm, and 471 nm assigned **to** $(^6H_{15/2} \rightarrow {}^4M_{17/2}, {}^6P_{3/2})$, $(^6H_{15/2} \rightarrow {}^6P_{7/2})$, $(^6H_{15/2} \rightarrow {}^4I_{11/2}, {}^6P_{5/2})$, $(^6H_{15/2} \rightarrow {}^4I_{13/2}, {}^4F_{7/2})$, $(^6H_{15/2} \rightarrow {}^4G_{11/2})$, $(^6H_{15/2} \rightarrow {}^4I_{15/2})$ **and** $(^6H_{15/2} \rightarrow {}^4F_{9/2})$ transitions of Dy^{3+} ions, respectively [2, 9]. It is concluded that the samples can effectively stimulate

Table 3 The Y/B ratio for present samples and compare them with other samples

Glass composition	Y/B 350 nm	Y/B 370 nm	Y/B 390 nm			Reference
lithium borosilicate glass 0.1Dy	1.11	0.97	1.06			P. w
lithium borosilicate glass 0.5	1.1	1.0	1.03			P. w
lithium borosilicate glass 1.0	1.11	1.03	1.05			P. w
lithium borosilicate glass 1.5	1.11	1.0	1.02			P. w
lithium borosilicate glass 2.0	1.11	0.97	1.02			P. w
fluoride-based bismuth phosphate 0.1Dy	1.856					[42]
fluoride-based bismuth phosphate 0.5Dy	1.942					[42]
fluoride-based bismuth phosphate 1.0Dy	1.978					[42]
fluoride-based bismuth phosphate 1.5Dy	1.978					[42]
fluoride-based bismuth phosphate 2.0Dy	1.918					[42]
Lithium borosilicate 0.5Dy	1.1	0.99	1.07			[23]
Lithium borosilicate 1.0Dy	1.11	1.01	1.06			[23]
Lithium borosilicate 2.50Dy	1.13	0.95	0.99			[23]
Lithium borosilicate 5.0Dy	1.1	1.01	0.98			[23]
Lithium borosilicate 10.0Dy	–	0.73	0.79			[23]
Alkali lead bismuth borate (K1Dy)			1.04			[58]
Alkali lead bismuth borate (Na1Dy)			1.07			[58]
Alkali lead bismuth borate (Ca1Dy)			1.08			[58]
Alkali lead bismuth borate (Sr1Dy)			1.18			[58]
Alkali lead bismuth borate (Ba1Dy)			1.15			[58]
Dy: bismuth zinc borate glasses			1.6			[59]
Dy: zinc-lithium- borotellurite glasses			1.093			[60]
Dy: yttrium calcium silicoborate glasses			1.141			[63]
Dy: fluoroaluminatetellurite			1.04			[64]
Lithium boro-tellurite: Dy	1.571					[65]
Calcium boro-tellurite: Dy	2.162					[65]
Zinc boro-tellurite: Dy	2.25					[65]
Barium boro-tellurite: Dy	1.285					[65]
Strontium boro-tellurite: Dy	1.761					[65]
doped magnesium zinc sulfophosphate glass: Dy	1.6					[86]
Bi2O3-B2O3-Ga2O3-GeO2-TeO2 0.5 Dy				1.06		[68]
Bi2O3-B2O3-Ga2O3-GeO2-TeO2 1.0 Dy				1.07		[68]
Bi2O3-B2O3-Ga2O3-GeO2-TeO2 1.5 Dy				1.13		[68]
Bi2O3-B2O3-Ga2O3-GeO2-TeO2 2.0 Dy				1.1		[68]
SiO2–B2O3–Al2O3–NaF–ZnF2: Dy 0.5	1.78					[30]
SiO2–B2O3–Al2O3–NaF–ZnF2: Dy 0.7	1.81					[30]
SiO2–B2O3–Al2O3–NaF–ZnF2: Dy 1.0	1.82					[30]
SiO2–B2O3–Al2O3–NaF–ZnF2: Dy 1.5	1.85					[30]
Sodium lead alumino borosilicate: Dy 0.5				1.063	385	[20]
Sodium lead alumino borosilicate: Dy 1.0				1.092		[20]
Sodium lead alumino borosilicate: Dy 1.5				1.088		[20]
Zinc alumino Bismuth Borate glasses: Dy10				1.18		[12]
Lithium tetraborate glasses: Dy8				1.019		[87]
Na2O–MgO–Bi2O3-B2O3: Dy0.1				1.68	390	[80]
Na2O–MgO–Bi2O3-B2O3: Dy0.5				1.76		[80]
Na2O–MgO–Bi2O3-B2O3: Dy1.0				1.85		[80]
Na2O–MgO–Bi2O3-B2O3: Dy1.5				1.89		[80]
Na2O–MgO–Bi2O3-B2O3: Dy2.0				1.76		[80]
Na2O–BaO–Bi2O3-B2O3 Dy0.1				1.91		[80]
Na2O–BaO–Bi2O3-B2O3 Dy0.5				1.85		[80]

Table 3 (continued)

Glass composition	Y/B 350 nm	Y/B 370 nm	Y/B 390 nm		Reference
Na2O–BaO–Bi2O3-B2O3 Dy1.0				1.86	[80]
Na2O–BaO–Bi2O3-B2O3 Dy1.5				2.04	[80]
Na2O–BaO–Bi2O3-B2O3 Dy2.0				1.95	[80]

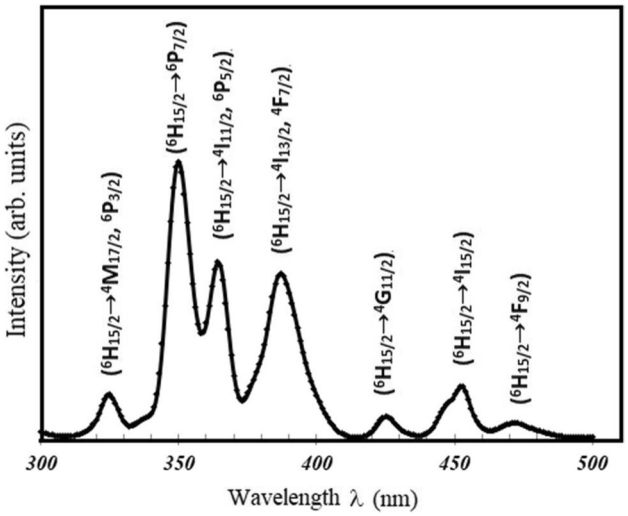

Fig. 7 Excitation spectra of a doped glass sample at a higher concentration of 1% Dy by observing the emission spectra at 575 nm

the range of ultraviolet (UV) light and near-ultraviolet (NUV) light to blue light. It can be used as commercial chips and Blue LED or GaN lamps because they emit an ideal phosphor in the 350–410 nm range [2, 9, 22].

The larger and broader peaks at 350 nm were utilized as the exciting energy of prepared glass samples, while the others at 370 nm and 390 nm were used to investigate the effect of different exciting energies on glass (Fig. 8).

In spectra of prepared glass samples excited at 350 nm, 370 nm, and 390 nm, two peaks at 484 nm and 574 nm ascribed **to $^4F_{15/2} \rightarrow {}^6H_{15/2}$ and $^4F_{15/2} \rightarrow {}^6H_{13/2}$** are shown in Fig. 8. The two reasons appear to be emissions. The first, levels above $^4F_{9/2}$, have low energy, allowing them to be close enough to release electrons via non-radiative relaxation.

The second factor is the high energy distance between the $^4F_{9/2}$ and the lower energy $^4F_{1/2}$ (7000 cm^{-1}), which allows it to absorb electrons at the $^4F_{9/2}$ level and emit them as radiative energy in the form of yellow and blue emissions at the lower level.

The blue emission expressed as the magnetic dipole (MD) doesn't affect the environment via the rule ($\Delta J = 0, \pm 1$ but $0 \leftrightarrow 0$ forbidden). The electric dipole (ED) represented by yellow emission is a hypersensitive transition with its surroundings via the rule ($\Delta J = 0, \pm 2$) [9].

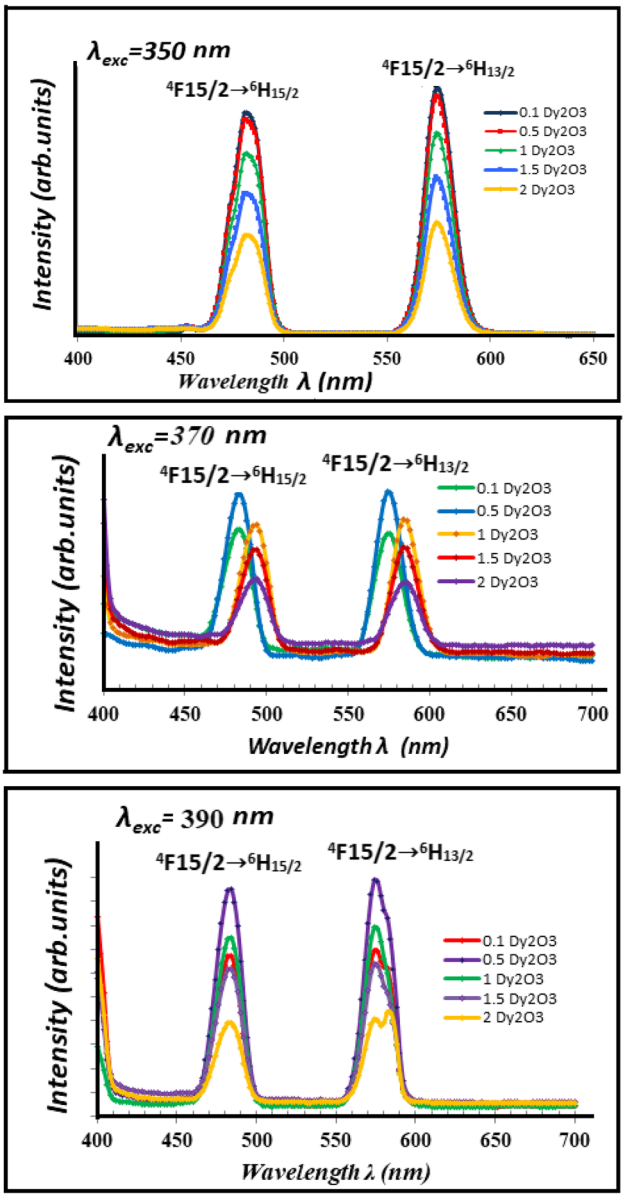

Fig. 8 Emission spectra of glass samples excited at 350, 370 and 390 nm

Figure 8 demonstrates that the peak's strength rises with Dy_2O_3 concentration up to 0.5, and then falls as quenching events in the glass samples are stimulated by 370 nm and 390 nm. The samples excited by 350 nm decrease from the composition of 0.1 mol% Dy_2O_3.

Table 4 Color coordinates (x, y) of Dy3 + doped glass samples under 350, 370 and 390 nm excitation comparison with other glass

Glass composition	λex 350 nm		λex 370 nm		λex 390 nm		CCT	CCT	CCT	Reference
	x	y	x	y	x	y				
lithium borosilicate glass 0.1Dy	0.33	0.38	0.31	0.33	0.34	0.36				P. w
lithium borosilicate glass 0.5	0.33	0.37	0.33	0.34	0.34	0.37				P. w
lithium borosilicate glass 1.0	0.33	0.37	0.33	0.34	0.34	0.37				P. w
lithium borosilicate glass 1.5	0.33	0.36	0.32	0.33	0.33	0.35				P. w
lithium borosilicate glass 2.0	0.32	0.36	0.32	0.33	0.34	0.35				P. w
fluoride-based bismuth phosphate 0.1Dy	0.342	0.396					5206			[42]
fluoride-based bismuth phosphate 0.5	0.341	0.397					5208			[42]
fluoride-based bismuth phosphate 1.0	0.331	0.355					5487			[42]
fluoride-based bismuth phosphate 1.5	0.336	0.378					4626			[42]
fluoride-based bismuth phosphate 2.0	0.358	0.369					4593			[42]
Li2O-BaO-Gd2O3- SiO2: Dy					0.332	0.347			5500	[15]
			λex450nm							
niobium phosphate glasses:0.5Dy			0.41	0.42			4344			[88]
ZnBiNaPSr oxyfluoride glasses Dy1.0			0.345	0.39			5115			[89]
magnesium-sodium-borotellurite glasses 0.05D					0.3607	0.4040			4682	[49]
magnesium-sodium-borotellurite glasses 0.5D					0.3716	0.4124			4433	[49]
magnesium-sodium-borotellurite glasses 1.0D					0.3681	0.413			4523	[49]
magnesium-sodium-borotellurite glasses 1.5D					0.3781	0.2407			4311	[49]
Lithium borosilicate 0.5Dy	0.34	0.36	0.32	0.33	0.34	0.35	5095	6046	5141	[23]
Lithium borosilicate 1.0Dy	0.36	0.37	0.32	0.34	0.34	0.37	4488	5733	5147	[23]
Lithium borosilicate 2.50Dy	0.34	0.36	0.31	0.32	0.34	0.35	4946	6474	4824	[23]
Lithium borosilicate 5.0Dy	0.35	0.31	0.31	0.31	0.39	0.36	4215	6621	3497	[23]
Lithium borosilicate 10.0Dy	–	-	0.31	0.30	0.32	0.31	–	6867	5942	[23]
Potassium lead bismuth borate (K1Dy)					0.386	0.401			4022	[58]
Sodium lead bismuth borate (Na1Dy)					0.397	0.427			3928	[58]
Calcium lead bismuth borate (Ca1Dy)					0.391	0.421			4022	[58]
Strontium lead bismuth borate (Sr1Dy)					0.351	0.415			4978	[58]
Barium lead bismuth borate (Ba1Dy)					0.333	0.383			5485	[58]
zinc telluro-fluoroborate glasses: Dy					0.354	0.407			4877	[90]
titania- fluorophosphate glasses: Dy					0.4	0.45			4006	[91]
ZrO2 – Na2O – B2O3 glasses: Dy					0.39	0.42			4039	[92]
B2O3–Al2O3–ZnF2–NaF/LiF oxyfluoride glasses: Dy					0.347	0.38			5016	[93]
Lithium boro-tellurite: Dy					0.323	0.359			5878	[65]
Calcium boro-tellurite: Dy					0.31	0.325			6672	[65]
Zinc boro-tellurite: Dy					0.339	0.349			5234	[65]
Barium boro-tellurite: Dy					0.326	0.345			5785	[65]
Strontium boro-tellurite: Dy					0.307	0.315			6982	[65]
doped magnesium zinc sulfophosphate glass: Dy					0.39	0.42			4039	[94]
					λex450	CCt				
Bi2O3-B2O3-Ga2O3-GeO2-TeO2 0.5 Dy					0.32	0.35	6195			[68]
Bi2O3-B2O3-Ga2O3-GeO2-TeO2 1.0 Dy					0.32	0.35	6051			[68]
Bi2O3-B2O3-Ga2O3-GeO2-TeO2 1.5 Dy					0.33	0.36	5723			[68]
Bi2O3-B2O3-Ga2O3-GeO2-TeO2 2.0 Dy					0.31	0.34	6355			[68]
SiO2–B2O3–Al2O3–NaF–ZnF2 0.5	0.389	0.435					4123			[30]
SiO2–B2O3–Al2O3–NaF–ZnF2 1.0	0.392	0.435					4061			[30]
SiO2–B2O3–Al2O3–NaF–ZnF2 1.5	0.393	0.439					4072			[30]
SiO2–B2O3–Al2O3–NaF–ZnF2 2.0	0.4	0.439					4022			[30]
Sodium lead alumino borosilicate Dy 0.5					0.34	0.38			5107	[20]

Table 4 (continued)

Glass composition	λex 350 nm		λex 370 nm		λex 390 nm		CCT	CCT	CCT	Reference
	x	y	x	y	x	y				
Sodium lead alumino borosilicate Dy 1.0					0.34	0.39			5271	[20]
Sodium lead alumino borosilicate Dy 1.5					0.34	0.39			5362	[20]
Zinc alumino Bismuth Borate glasses: Dy					0.31	0.31			—	[12]
sodium-aluminum-phosphate glasses: Dy					0.44	0.44			—	[95]
Li2B4O7 glasses: Dy					0.35	0.38			—	[87]
calcium tungstate: Dy					0.34	0.35			5288	[96]
Na2O–MgO–Bi2O3-B2O3: Dy0.1					0.38	0.41			4201	[80]
Na2O–MgO–Bi2O3-B2O3: Dy 0.5					0.385	0.416			4133	[80]
Na2O–MgO–Bi2O3-B2O3: Dy 1.0					0.388	0.419			4082	[80]
Na2O–MgO–Bi2O3-B2O3: Dy 1.5					0.39	0.42			4035	[80]
Na2O–MgO–Bi2O3-B2O3: Dy 2.0					0.384	0.416			4137	[80]
Na2O–BaO–Bi2O3-B2O3: Dy 0.1					0.394	0.421			3963	[80]
Na2O–BaO–Bi2O3-B2O3: Dy 0.5					0.388	0.418			4067	[80]
Na2O–BaO–Bi2O3-B2O3: Dy 1.0					0.391	0.421			4014	[80]
Na2O–BaO–Bi2O3-B2O3: Dy 1.5					0.394	0.424			3977	[80]
Na2O–BaO–Bi2O3-B2O3: Dy 2.0					0.391	0.421			4017	[80]

The quenching phenomena are formed by increasing the Dy_2O_3 concentration, which reduces the intermolecular distance between the molecules. It causes the Dy^{3+} ions to close together, allowing excitation energy to be transmitted between surrounding rare-earth ions, resulting in a reduction in emission intensity [7] and an increase in non-radiative energy via the cross-relaxation and resonant energy channels [19].

In numerous references [4, 8, 9, 21, 22], the radiative transition created by photons and the non-radiative transition formed by phonons in the Dy emission.

The symmetry around Dy can be seen in the ratio between ED and MD [22, 40]. The higher the ED emission, the more asymmetric the glass composition is, and the Dy ions are in the low symmetry center. The increased covalency between Dy and O ions is shown by the high value of the Y/B (yellow emission/ blue emission) ratio found in Table 3 [15]. The laser's white light emission is predicted by a Y/B value greater than unity [4]. With the different Dy_2O_3 concentrations, Table 3 shows a less significant difference in the Y/B ratio. It is caused by a disparity in sensitivity intensity.

Table 3 compares the Y/B ratio of the glass samples under investigation to that of other glass systems. In the creation of white light, a specific emission intensity ratio of yellow to blue (Y/B) is important. If the Y/B ratio is one, it will produce pristine white light.

The acquired Y/B ratios for the glass samples under investigation ranged from 0.9 to 1.1, as shown in Table 3.

Also, note from Table 3 that adding Dy^{3+} ions to the host (Present work) or at the expense of the former component (Borate) of the glass (reference 13) does not change in the properties studied.

With an excitation wavelength of 350, 370, or 390 nm, the Y/B ratio is virtually equal to unity, making it the finest choice for warm white light materials and the production of WLEDs from these glasses, which are ideal for emitting white color and various photonic applications.

As stated in Table 4, this result was compared to other produced glass samples.

Emission spectroscopy measurements with a CIE 1931 chromatogram, which is shown as a mapping that predicts the commonly achieved light coordination point of monochromatic light [1, 40] ($\Delta\lambda \rightarrow 0$) located around the chromaticity peripheral, are used to characterize luminance intensity.

The CIE diagram of prepared glass samples with various Dy_2O_3 concentrations and excitations migrating to the center as the source spectral bandwidth widens is depicted in Fig. 9.

Any variation in Dy concentration and excitation wavelength could impact the (x, y) parameter [9], which identified all samples around a perfect white light (0.33, 0.33) [1, 7] based on the co-oriented values obtained.

CCT analyzed the quality of emitted light by measuring illumination appearance and white light chromaticity.

The CCT of glass samples in the 6000-6500 K > 4000 K range utilized as the warm white light is shown in Fig. 9 [4, 7, 22].

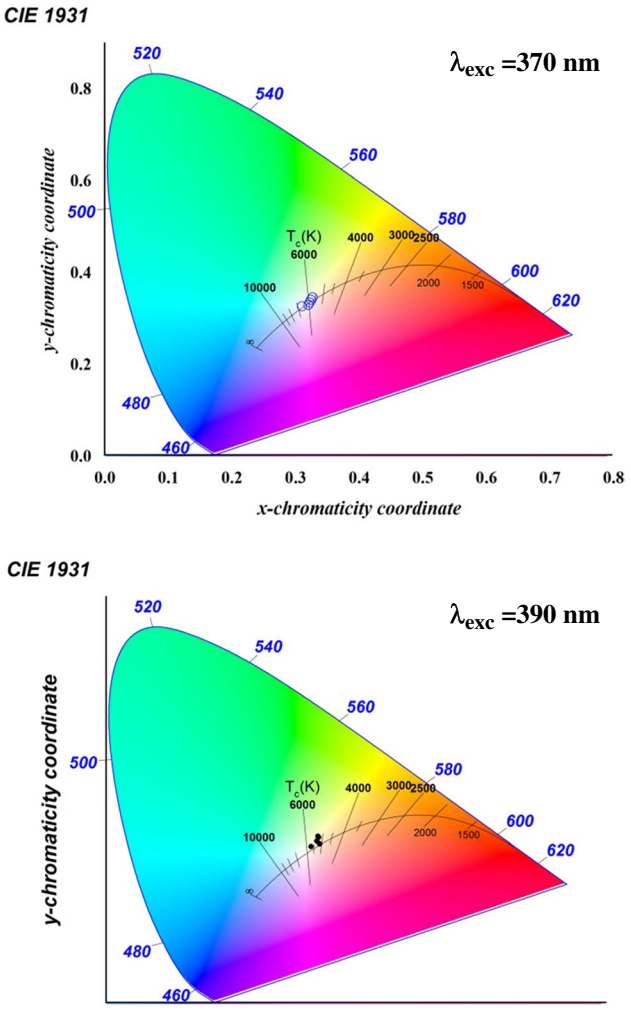

Fig. 9 The CIE diagram of prepared glass samples with different Dy concentration and different excitation energy

4 Conclusions

Lithium borosilicate glasses doped with different concentrations of Dysprosium oxide were investigated using a spectroscopic technique such as an XRD diffractometer, FTIR, optical absorption, and photoluminescence (excitation & emission) properties were studied for Dy^{3+} doped glasses. The Judd–Ofelt parameter calculated for reported glasses follows the trend $\Omega2 > \Omega6 > \Omega4$ and shows that the Dy-O bond's covalence with the host glass is more asymmetric. The luminescence spectrum exhibits two peaks corresponding to the transitions $^4F_{9/2} \rightarrow {}^6H_{15/2}$ (blue) and $^4F_{9/2} \rightarrow {}^6H_{13/2}$ (yellow), in which the white light transition is dominant. Based on the findings, it appears to be a viable option for laser-active medium and lighting device applications.

Acknowledgements I.Kashif thanks Prof. Dr. A. M. Sanad for his support throughout my scientific career during his stay with us.

Author Contributio All authors contributed to the study conception and design. Material preparation, data collection and analysis were performed by [A. Ratep] and [I. Kashif]. All authors commented on previous versions of the manuscript. All authors read and approved the final manuscript.

We, the authors of this paper, agree to send it to your journal and that Prof. I. Kashif is the corresponding author for submitting the research and addressing the journal.

Funding The authors declare that no funds, grants, or other support were received during the preparation of this manuscript.

Data Availability The data that support the findings of this study are available from the corresponding author upon reasonable request.

Declarations

Competing interests The authors declare no competing interests.

Conflict of Interest All authors listed have made a significant contribution to the research reported and have read and approved the submitted manuscript.
The authors declare that they have no known competing financial interests or personal relationships that could have appeared to influence the work reported in this paper.
All authors have seen and approved the final version of the manuscript being submitted.—The article is the original work,—hasn't received prior publication and isn't under consideration for publication elsewhere.

Competing Interests The authors declare that they have no known competing financial interests or personal relationships that could have appeared to influence the work reported in this paper.

Consent for Publication All authors agree with the review of this paper in this journal

References

1. Damak K, Yousef ES, Rüssel C, Maâlej R (2014) J Quant Spectrosc Radiat Transf 134:55
2. Bergh A, Craford G, Duggal A, Haitz R (2001) Phys Today 54:42
3. Kohale RL, Dhoble SJ (2013) J Lumin 138:153
4. Lakshminarayana G, Baki SO, Lira A, Kityk IV, Caldiño U, Kaky KM et al (2017) J Lumin 186:283
5. Sun Z, Ci, Qin Q S, Sun M, Jiang X, Zhang X, Wang Y (2014) Phys Chem Chem Phys 16:11597
6. Lin CC, Meijerink A, Liu R-S (2016) J Phys Chem Lett 7:495
7. Pawar PP, Munishwar SR, Gautam S, Gedam RS (2017) J Lumin 183:79
8. Mishra L, Sharma A, Vishwakarma AK, Jha K, Jayasimhadri M, Ratnam BV, Jang K, Rao AS, Sinha RK (2016) J Lumin 169:121
9. Mahamuda SK, Swapna K, Packiyaraj P, Rao AS, Prakash GV (2014) J Lumin 153:382
10. Azizan SA, Hashim S, Razak NA, Mhareb MHA, Alajerami YSM, Tamchek N (2014) J Mol Struct 1076:20
11. Zhao C-J, Cai J-L, Li R-Y, Tie S-L, Wan X, Shen J-Y (2012) J Non-Cryst Solids 358:604
12. Swapna K, Mahamuda Sk, Rao A S, Jayasimhadri M, Sasikala T, Moorthy L R (2013) J Lumin 139:119

13. Chen Q, Dai N, Liu Z, Chu y, Ye B, Li H et al (2014) Appl Phys A Mater Sci Process 115:1159
14. Edukondalu A, Purnima M, Srinivasy Ch, Sripathi T, Awasthi AM, Rahman S, Kumar KS (2012) J Non-Cryst Solids 358:2581
15. Khan I, Rooh G, Rajaramakrishna R, Srisittipokakun N, Wongdeeying C, Kiwsakunkran N, Kim HJ, Kaewkhao J, Tuscharoen S (2019) J Alloys Compd 774:244
16. Dwivedi Y, Rai SB (2009) Opt Mater 31:1472
17. Alajerami YSM, Hashim S, Hassan WMSW, Ramli AT, Kasim A (2012) Physica B 407:2398
18. Vijaya N, Kumar KU, Jayasankar CK (2013) Spectrochim Acta Part A Mol Biomol Spectrosc 113:145
19. Rajesh D, Ratnakaram YC, Seshadri M, Balakrishna A, Krishna TS (2012) J Lumin 132:841
20. Babu KV, Cole S (2018) Ceram Int 44:9080
21. Chimalawong P, Kirdsiri K, Kaewkhao J, Limsuwan P (2012) Procedia Engineering 32:690
22. Kaur R, Bhatia V, Kumar D, Rao SMD, Singh SP, Kumar A (2019) Results Phys 12:827
23. Kashif I and Ratep A (2021) Accepted in J the Spanish Ceramic and Glass Society Cerámica y Vidrio
24. Kaur R, Singh S, Pandey OP (2013) J Mol Struct 1049:409
25. Lai Y, Zeng Y, Tang X, Zhang H, Han J, Su H (2016) RSC Adv 6:93722
26. Shaaban KS, El-Maaref AA, Abdelawwad M, SaddeekY B, Wilke H, Hillmer H (2018) J Lumin 196:477
27. Goyal P, Sharma YK, Pal S, Bind UC, Huang SC, Chung SL (2017) J Lumin 192:1227
28. Moustafa MG, Morshidy H, Mohamed AR, El-Okr MM (2019) J Non-Cryst Solids 517:9
29. Kaur M, Singh A, Thakur V, Singh L (2016) Opt Mater (Amst) 53:181
30. Monisha M, D'Souza AN, Hegde V, Prabhu NS, Sayyed MI, Lakshminarayana G et al (2020) Curr Appl Phys 20:1207
31. Ramteke DD, Kroon RE, Swart HC (2017) J Non-Cryst Solids 457:157
32. Ramteke DD, Gedam RS, Swart HC (2018) Phys B Condens Matter 535:194
33. Kashif I, Ratep A (2017) Opt Quantum Electron 49:231
34. Mhareb MHA, Almessiere MA, Sayyed MI, Alajerami YSM (2019) Optik (Stuttg) 182:821
35. Prabhu NS, Hegde V, Sayyed MI, Şakar E, Kamath SD (2019) Infrared Phys Technol 98:7
36. Rao KV, Babu S, Venkataiah G, Ratnakaram YC (2015) J Mol Struct 1094:274
37. Kumar JS, Pavani K, Babu AM, Giri NK, Rai SB, Moorthy LR (2010) J Lumin 130:1916
38. El-Maaref A A, Shaaban K S, Abdelawwad M, Saddeek Y B (2017) Opt Mater (Amst) 72:169
39. Monisha M, Mazumder N, Lakshminarayana G, Mandal S, Kamath SD (2020) Ceram Int 47:598
40. Balakrishna A, Rajesh D, Ratnakaram YC (2012) J Lumin 132:2984
41. Iezid M, Goumeidane F, Abidi A, Poulain M, Legouera M, Prasad PS et al (2021) J Opt Mater 120:111422
42. Babu PR, Rajesh M, Sushma NJ, Kavaz E, Raju BDP (2021) J Opt Mater 122:111725
43. Jamalaiah BC, Kumar JS, Suhasini T, Jang K, Lee HS, Choi H, Moorthy LR (2009) J Alloys Compd 474:382
44. Ravi O, Reddy CM, Reddy BS, Raju BDP (2014) Opt Commun 312:263
45. Saleem SA, Jamalaiah BC, Jayasimhadri M, Rao AS, Jang K, Moorthy LR (2011) J Quant Spectrosc Radiat Trans 112:78
46. Hormadaly J, Reisfeld R (1979) J Non-Cryst Solids 30:337
47. Babu S, Prasad VR, Rajesh D, Ratnakaram YC (2015) J Mol Struct 1080:153
48. Damodaraiah S, Prasad VR, Babu S, Ratnakaram YC (2017) J Opt Mater 67:14
49. Gonzalez-Suarez E, Lira A, Mariscal-Becerra L, Meza-Rocha AN, Caldino U (2022) Opt Mater 123:111930
50. Kıbrısl O, Ersundu AE, Ersundu MC (2019) J Non-Cryst Solids 513:125
51. Gökce M, Kocyigit D (2019) Opt Mater (Amst) 89:568
52. Kumar A, Rai D K, Rai S B (2002) Spectrochim Acta – Part AMol Biomol Spectrosc 58:3067
53. Ichoja A, Hashim S, Ghoshal SK, Hashim IH, Omar RS (2018) J Rare Earths 36:1264
54. Naick BN, Damodaraiah S, Prasad VR, Lakshmi RPV, Ratnakaram YC (2019) Optik (Stuttg) 192:162980
55. Babu MR, Rao NM, Babu AM, Jaidass N, Moorthy CK, Moorthy LR (2016) Optik (Stuttg) 127:3121
56. Jupri SA, Ghoshal SK, Omar MF, Yusof NN (2018) J Alloys Compd 753:446
57. Suresh B, Zhydachevskii Y, Brik MG, Suchocki A, Reddy MS, Michałand NP (2016) J Alloys Compd 683:114
58. Divina R, Teresa PE, Marimuthu K (2021) J Alloys Compd 883:160845
59. Shanmugavelu B, Kumar VVRK (2014) J Lumin 146:358
60. Malge A, Sankarappa T, Sujatha T, Devidas G B, PAzeem P A (2020) Opt Mater 109:110282
61. Karki S, Kesavulu CR, Kim HJ, Kaewkhao J, Chanthima N, Kothan S et al (2019) J Noncryst Solids 521:119483
62. George H, Deopa N, Kaur S, Prasad A, Sreenivasulu M, Jayasimhadri M, Rao AS (2019) J Lumin 215:116693
63. Kesavulu C R, kim H J, Lee S W, Kaewkhao J, Chanthima N, Tariwong Y (2017) J Alloy Compd 726:1062
64. Huang F, Hu L, Chen D (2014) Ceram Int 40:12869
65. Teresa PE, Divina R, Naseer KA, Marimuthu K (2022) Optik - International Journal for Light and Electron Optics 259:169024
66. Kaur A, Khanna A, Gonzalez-Barriuso M, Gonzalez F (2021) J Mater Sci Mater Electron 32:17266
67. Liu R, Wang D, Chen M, Liu L, Zhou Y, Zeng F, Su Z (2021) J Lumin 237:118180
68. Kashif I, Ratep A (2022) Mater Sci Eng, B 275:115488
69. Lodi TA, Dantas NF, Gonçalves TS, De Camargo ASS, Pedrochi F, Steimacher A (2019) J Lumin 207:378
70. Karthikeyan P, Arunkumar S, Annapoorani K, Marimuthu K (2018) Spectrochim Acta Part A Mol Biomol Spectrosc 193:422
71. Annapoorani K, Karthikeyan P, Basavapoornima C, Marimuthu K (2017) J Non-Cryst Solids 476:128
72. Sasikala T, Jayasimhadri M, Mahamuda S, Rao AS, Swapna K, Moorthy LR (2013) J Lumin 139:119
73. Kumar MVV, Jamalaiah BC, Gopal KR, Reddy RR (2012) J Lumin 132:86
74. Ratnakaram YC, Naidu DT, Vijayakumar A, Rao JL (2012) J Non-Cryst Solids 358:204
75. Ahamed SdZA, Reddy CM, Raju BDP (2013) Opt Mater 35:1385
76. Kiran N, A Kumar A S (2013) J Mol Struct 1054:6
77. Kesavulu CR, Jayasankar CK (2011) Mater Chem Phys 130:1078
78. Arunkumar S, Venkataiah G, Marimuthu K (2015) Acta Part A: Mol Bimol 136:1684
79. Rao GV, Jayasankar CK (2015) J Mol Struct 1084:182
80. Zaman F, Srisittipokakun N, Rooh G, Khattak SA, Kaewkhao J, Rani M, Kim HJ (2021) Opt Mater 119:111308
81. Zaman F, Kaewkhao J, Srisittipokakun N, Wantana N, Kim HJ, Rooh G (2016) Opt Mater 55:136
82. Ryba-Romanowski W, Dominiak-Dzik G, Solarz P, Lisiecki R (2009) Opt Mater 31:1547
83. Rayappan IA, Marimuthu K, Babu SS, Sivaraman M (2010) J Lumin 130:2407

84. Pisarska J (2009) J Phys Condens Matter 21:285101
85. Adam JL, Docq AD, Lucas J (1988) J Solid State Chem 75:403
86. Eevon C, Halimah MK, Zakaria A, Azurahanim CAC, Azlan MN, Faznny MF (2016) Results Phys 6:761
87. Sun X-Y, Wu S, Liu Xi, Gao P, Huang S-M (2013) J Non-Cryst Solids 368:51
88. Srihari T, Jayasankar CK (2017) Opt Mater 69:87
89. Raju DS, Raju BDP, Bindu SH, Latha MH, Krishna JS, Krishna VV et al (2021) Mater Today: Proceedings 47:4364
90. Suthanthirakumar P, Marimuthu K (2016) J Mol Struct 1125:443
91. Ravi N, Neelima G, Nallabala NKR, Kummara VK, Ravanamma R, Reddy VJ et al (2020) Opt Mater 111:110593
92. Roopa BE (2021) J Non- Cryst Solids 551:12039
93. Lakshminarayana G, Vighnesh KR, Prabhu NS, Lee D-E, Yoon J, Park T et al (2020) Opt Mater 108:110186
94. Ahmadi F, Hussin R, Ghoshal SK (2018) J Non-Cryst Solids 499:131
95. Reddy AA, Sekhar MC, Pradeesh K, Babu SS, Prakash GV (2018) J Mater Sci 46:2018
96. Ambast AK, Goutam J, Som S, Sharma SK (2014) Spectrochim. Acta Part A: Mol Biol Mol Spectrosc 122:93